A Comparative Study of Prediction Techniques for Supersonic Missile Aerodynamic Coefficients

Loai A. El-Mahdy
Mahmoud Y. M. Ahmed
Osama K. Mahmoud
Omar E. Abdel-Hameed
Aerospace Department, Military Technical College, Cairo, Egypt

ABSTRACT

Evaluating the aerodynamic coefficients of flying vehicles such as missiles is a key step in their design and development procedures. In practice, the aerodynamic coefficients can be estimated using experimental measurements, numerical simulations, or using empirical and semi-empirical engineering tools. In the present paper, these three approaches are compared in the context of examining the aerodynamic coefficients of a fin-stabilized tactical missile. Supersonic flight conditions up to Mach 4 at incidence up to 18 degrees are considered. Lift and drag coefficients as well as the centre of pressure locations based on the three approaches are compared. The flow features around the missile are explored based on the numerical simulations.

Keywords: *Missile Aerodynamics; CFD; Wind Tunnel; Aerodynamic Coefficients; Supersonic Missile.*

Introduction

Throughout regular design and development routine of flying vehicles, understanding and evaluating the aerodynamic characteristics of these vehicles is one crucial step. In the conceptual design steps, empirical and semi-empirical tools are implemented to provide quick yet less accurate results. As the design process evolves towards the final design, higher fidelity tools such as computational and experimental techniques are applied for more accurate results.

In the framework of a research conducted by the authors to enhance an existing supersonic missile system, the missile airframe is modified. The

_____

aerodynamic coefficients of the modified missile are measured experimentally on a 1:16 model in a wind tunnel. In addition to better understanding the aerodynamic features of the modified airframe, the experimental measurements have shown some phenomena that needed to be confirmed using approaches other than the experimental one. Since the missile airframe is modified, its aerodynamic coefficients are not available especially, indeed, in the open literature. The present paper is devoted to presenting the findings of the comparative study on the different predictive approaches of the missile aerodynamics coefficients.

The aspects of the missile aerodynamics have been extensively studied by the researchers over decades and still draw the attention of researchers. To avoid lengthy and irrelevant survey, the focus here is made to survey from previous comparative studies of different predictive techniques. Experimental, empirical, and computational approaches were compared in a huge body of studies. Empirical and experimental approaches were compared in [1-13] whereas in [14-22], computational results were compared with experimental measurements. Computational techniques were also compared with empirical ones in [23].Comparative studies aggregating the three approaches were only conducted by Rosema el al. [24] who implemented the three approaches in a comparative study on the aerodynamic coefficients of several missiles with strakes.

The main objective of the present study is to explore and confirm the aerodynamic characteristics of a conventional tactical missile at high Mach numbers and high angles of attack. The findings of the experimental, computational, and empirical approaches are compared and presented as a contribution to the available database for researchers. It is also desired to assess the validity of an empirical code developed by the research group. The modified missile configuration under investigation is a cone-cylinder equipped with four trapezoidal stabilizing fins and the freestream Mach number varies from 1.5 to 4 at incidence angle varying from 4 to 18. The ranges of Mach number and angles of attack represent the real flight conditions of the modified missile in concern. The variation of the lift and drag coefficients and the centre of pressure location and the flowfield structure around the missile are considered. The commercial CFD solver ANSYS [25] is utilized as the computational tool whereas a research code developed by the authors is implemented as the semi-empirical tool. Data from a set of own experimental wind tunnel measurements are used for comparison. The case study and the approach of study are explained in detail in the next section followed by the discussion of the key results. The paper finalizes by the addressing the main conclusions.

Case Study and Methodology

The model that has been tested in the wind tunnel experiments is a 1:16 scaled missile body configuration. It is composed of cone-cylinder body, two outer conduits, and four fins. The model has a total length and caliber of 551.25 mm and 34 mm, respectively. The sketch of the model configuration is shown in Figure 1.
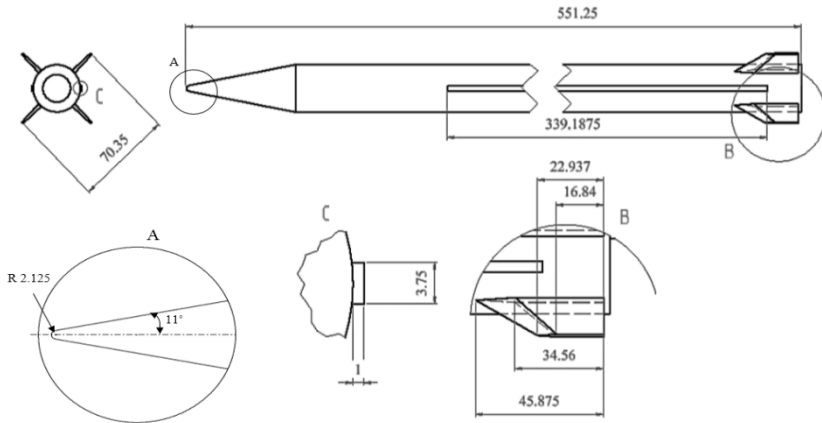

Figure 1: Model configuration

Wind tunnel data

Comprehensive experimental wind tunnel tests [26] have been conducted to estimate the aerodynamic characteristics of the model shown above. The model is tested in a tri-sonic wind tunnel which test section dimensions are 0.6×0.6 meters and its length is 1.575m. The test conditions are variable from Mach 0.4 to 4.45, the corresponding Reynolds number of the flow at the test section inlet varies from 8.7×10^6 to 26.5×10^6 such that the reference length is the total model length. A conventional attack angle mechanism can change the attack angle in the range of $-15°{\sim}38°$. The aerodynamic loads on the model are directly measured using a sting balance that is internally fitted in the base of the model that is placed in the test section with fins at the x-orientation.

Based on the measured loads, the aerodynamic coefficients are calculated by taking the reference length and area of 0.55125 m and 0.0009079 m^2, respectively. The accuracy of recorded data in measurements of the aerodynamic loads is maintained within $\pm1\%$ of their nominal values.

Numerical Simulation

A computational domain identical to the test section of the wind tunnel in the experiments is constructed so as to exactly replicate the experimental test conditions. The domain has the same dimension as the test section. Since only the incidence angle is considered, the flow around the model is pitch-plane symmetric. Thus, only half 3D domains are constructed, as shown in Figure 2.
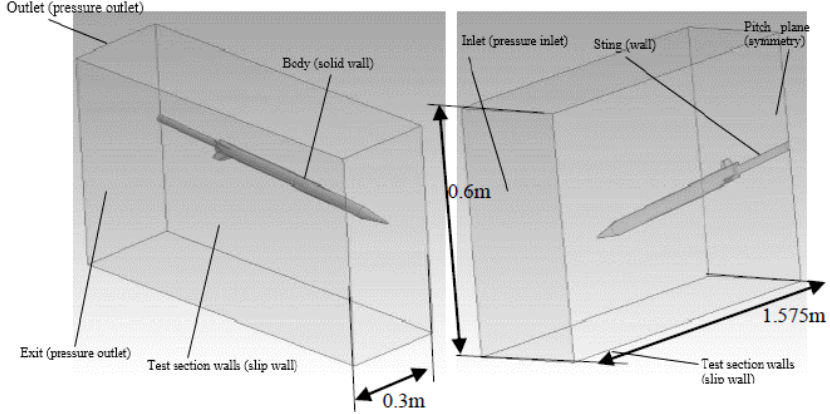

Figure 2: Boundaries of the bounded domain and their definitions

The upstream boundary of the domain is set to be pressure inlet. For this boundary type, the gauge total pressure and the total temperature are defined as in the tunnel experimental data. The downstream boundary is defined as pressure outlet where the values of the gauge pressure and the total temperature are specified. The pitch plane is defined as symmetry plane with zero normal gradients of the flow properties. All the surfaces of the model and the sting are defined as non-slip walls. The wind tunnel walls are defined as slip walls on which no boundary layer is created numerically. Domain boundary definitions are shown in Figure 2.

The domain is discretized using an unstructured tetrahedral grid. The quality of the generated grid is enhanced by applying successively two scoping methods; the body element sizing then the sphere of influence sizing. Body element sizing yields a clustered fine grid on the body surface only whereas the sphere of influence is drawn in the areas of the domain where the shock and expansion waves take place. Five spheres of influence are drawn eventually yielding a nearly feature-aligned grid (the thick circles in Figure mark the spheres of influence). A grid sensitivity check is applied to the grid. A grid with 1825562 cells is found to yield a grid-independent prediction of the aerodynamic coefficients.
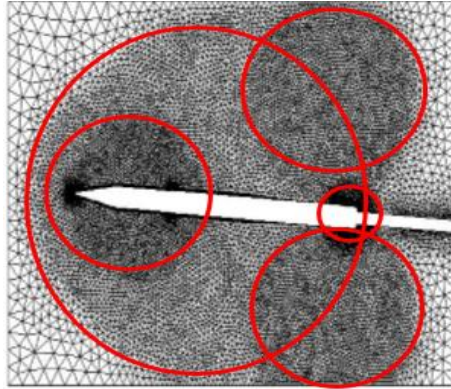
Figure 3: Domain discretization using sphere of influence scoping method

Since the CFD simulations are designed to simulate the flow through the wind tunnel test section, the incoming flow is made normal to the inlet boundary. The model angle of attack is introduced by making the model inclined with respect to the domain. Hence, for each angle of attack, a unique computational domain is created and discretized; the same grid refinement approach is adopted for all domains. To keep the simulations within the available limited computational budget and resources, it was decided to specify only four angles of attack that can be representative for the entire range of incidence angles in concern from low (4º) to moderate (10º, 14º) to high (18º). The selected angles of attack are expected to be sufficient to capture the trend of variation of aerodynamic features with incidence.

ANSYS FLUENT is a commercial CFD code which uses a cell-centered finite volume method and has been proven to work well for different flow regimes around missiles. The double-precision implicit density-based steady solver available in the solver is implemented in the present simulations along with a second-order special discretization scheme. Air is treated as ideal gas and Spalart-Allmaras turbulence model is implemented. The numerical simulation is said to converge once the iterations residuals drops below 1×10^5 while maintaining an invariable value of a physical criterion (taken here as the total drag coefficient on the model).

Semi-empirical prediction code

Missile Aerodynamics Code, MAC [27] is an aerodynamic prediction software that has been developed by the research group. It is specially designed to estimate the aerodynamic characteristics of winged and un-winged flying bodies with two sets of four-panel wings at 90º to each other. The concept depends on using experimental and theoretical data of standard body and panel

shapes which are known to an acceptable degree of accuracy [28-33] for calculating the aerodynamic characteristics of considered combination using the component build-up technique. The software calculates all aerodynamic coefficients and characteristics needed for determination of the flying body performances and flying qualities. The structure of the code that is written in MATLAB is composed of 39 subroutines. They are categorized into four groups. The geometry group handles all geometric inputs of the missile and calculates all geometric parameters necessary for calculations such as body surface areas, panels areas, etc. this set also includes a subroutine to calculate the atmospheric properties based on the input flight altitude and speed. The second set of subroutines estimate the missile drag. It includes subroutines to estimate the drag components (pressure, wave, skin friction, induced drag, etc.) on each of the missile airframe components. The total drag is calculated as the algebraic sum of all drag components. The thirst set includes lift and moment estimation subroutines. The individual lift and moments of each of the missile components are estimated. The overall missile lift and moments coefficients are calculated taking the interferences among missile body components into consideration. The last set of subroutines estimates the aerodynamic derivatives of the missile with respect to flight parameters.

Results and Discussions

Variation of the Total Lift Coefficient with the Freestream Conditions

The dependence of model lift coefficient on the freestream conditions is illustrated in the set of figures below; each for a value of freestream Mach number.
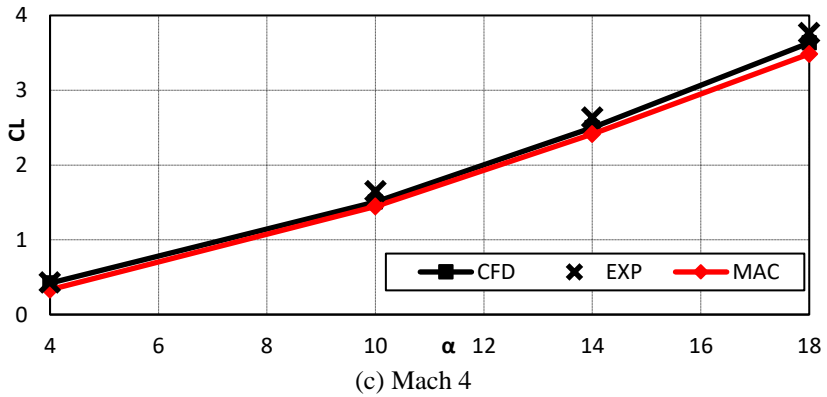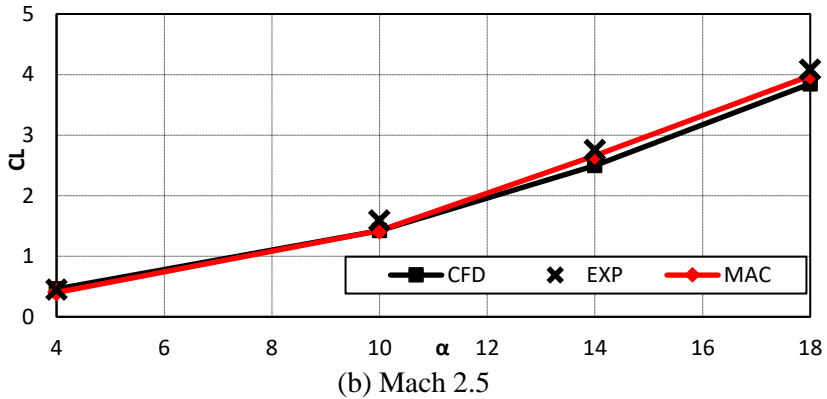

(a) Mach 1.5

(b) Mach 2.5

(c) Mach 4
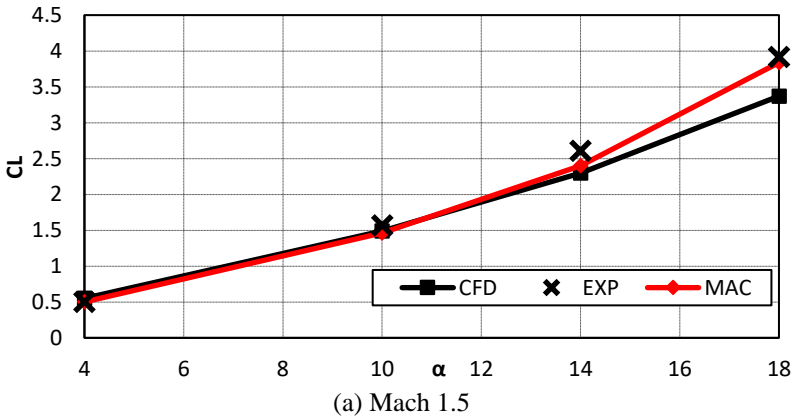
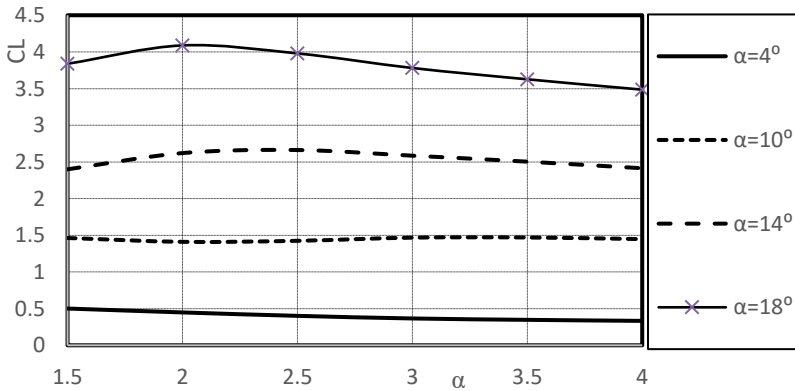Figure 4: Variation of lift coefficient with incidence

For all Mach numbers, similar to drag coefficient, the measured lift coefficient increases with the increase in the angle of attack. The curves show coherence of the computational and analytical results to the experimental measured behavior with very small error values at low incidence (4°) and higher ones at high incidences (14°). At extreme conditions namely, high Mach (Mach 4) and incidence (14°), CFD simulations results show better accuracy compared with those of the empirical tool. Figure brings together the dependence of the model lift coefficient with the freestream conditions, Mach and incidence values as estimated experimentally, numerically, and empirically. Clearly, lift coefficient is more sensitive to variation of incidence angle than that of the freestream Mach value.
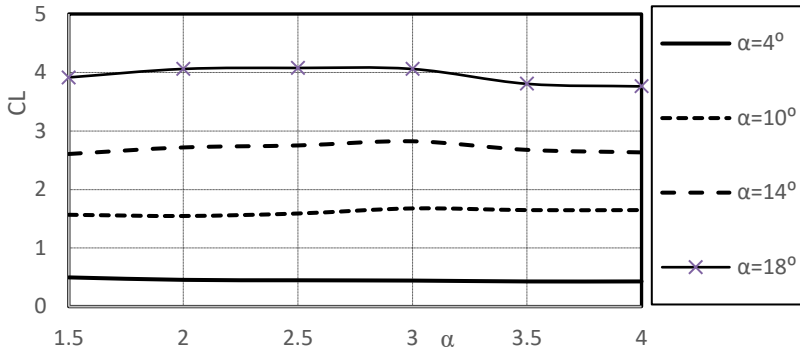
(a) Experiments
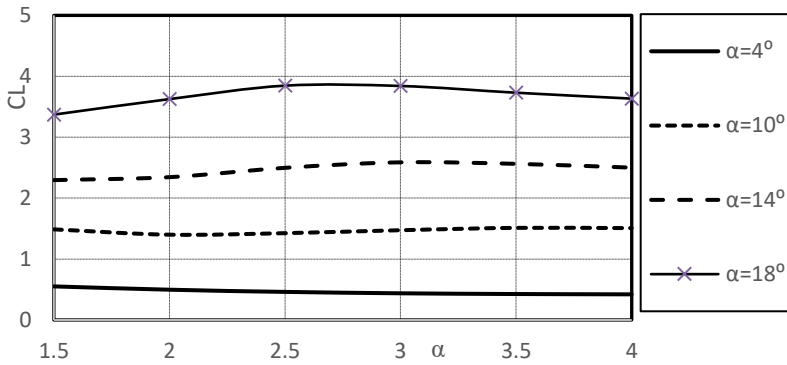
(b) CFD

(c) MAC

Figure 5: Variation of lift coefficient with the Mach number at different
angles of attack

Variation of the Total Drag Coefficient with the Freestream Conditions
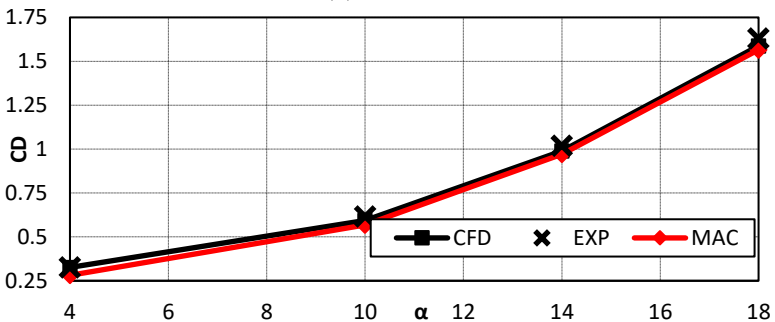
The dependence of the total drag coefficient of the model with the freestream conditions is illustrated in the set of figure below. In these figures, the variations of the experimental, numerical, and empirical results of total drag coefficient with incidence are compared for each value of Mach number.
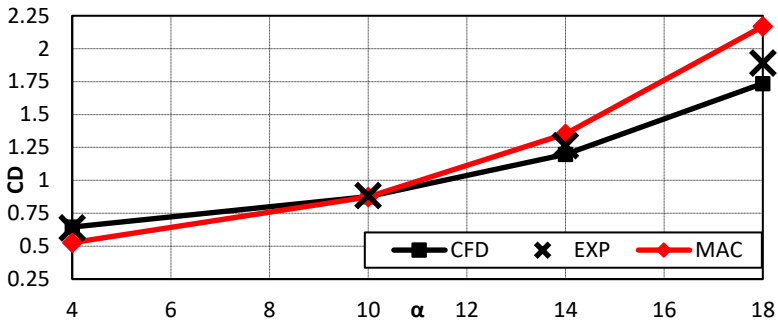
(a) Mach 1.5
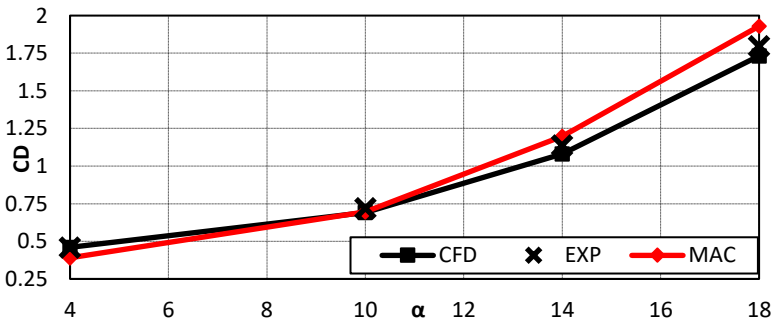
(b) Mach 2.5

(c) Mach 4

Figure 6: Variation of total drag coefficient with incidence

Closely examining the figure above shows that At 4º incidence, the drag has its minimum values for all Mach numbers. Drag decreases slightly with the increase in Mach value while it increases considerably with the incidence angle. As the incidence increases, the slope of this dependence increases monotonically. Generally, the rise in drag with the incidence angle shows a steep trend for α>10º. On average, the drag increases by about 52% as incidence increases from 4º to 10º. The percentage of drag rise increases by 56% then 58% as the incidence angle increases from 10º to 14º then to 18º. Compared with experimental values, the trend of results is better captured by CFD simulation than that given by empirical technique. This accuracy is more pronounced at higher Mach values than that at lower ones. The accuracy of MAC results is higher at incidence angles below 10º and improves at higher Mach values.

Figure 7 aggregates the dependence of CD on the freestream conditions namely, Mach number and incidence angle as estimated experimentally, computationally, and analytically. It is clear that the drag is more sensitive to the variation of incidence angle than to that of the free stream Mach number. The sensitivity of drag value with respect to incidence and Mach is measured by the change in drag value per unit change in incidence and Mach, respectively. For instance, from Figure 5a, the drag coefficient increases from 0.63 to 1.9 as the incidence angle increases from 4 to 18 (for Mach 1.5). The rise in drag becomes more pronounced with the increase in incidence. On average, the drag coefficient value increases by 14.4% per unit increase in incidence angle. In contrast, the drag coefficient drops from 1.9 to 1.63 as the Mach value increases from 1.5 to 4 (for 18º incidence). This corresponds to an average drop by 5.6% per unit increase in Mach value. Based on this estimation, the drag is said to be more sensitive to incidence than to Mach value.
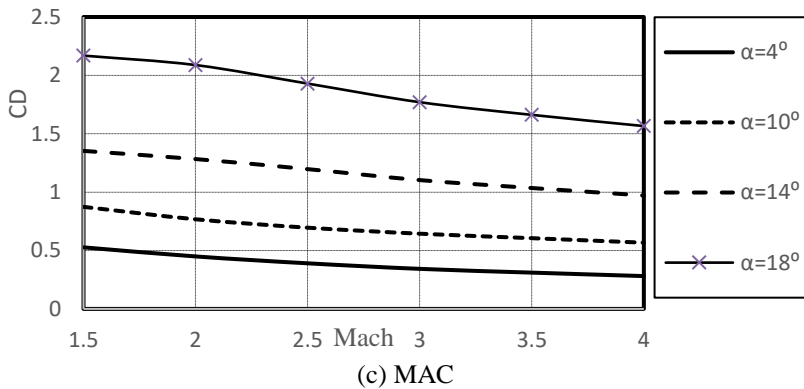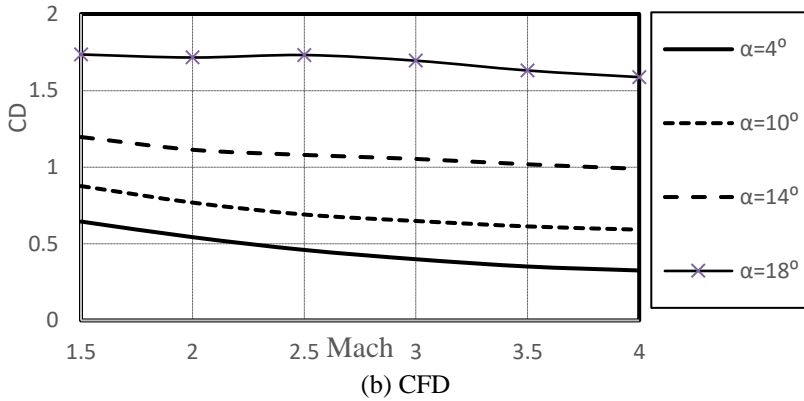

(a) Experiments

(b) CFD

(c) MAC
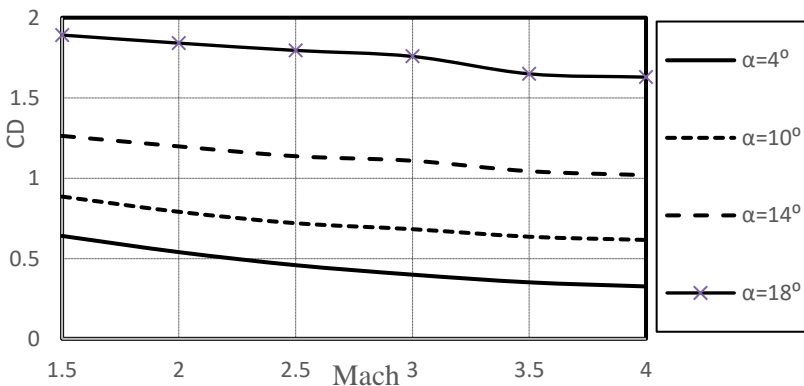
Figure 7: Change of the drag coefficient with the Mach number at different angles of attack

Variation of the Centre of Pressure Position with the Freestream Conditions

The centre of pressure of the missile is the point of action of the resultant aerodynamic forces acting on it, Figure 8. In experiments, it is calculated by dividing the measured pitching moment coefficient (about the model gravity centre) by the measured normal force coefficient. The distance to the pressure centre is then measured with respect to a fixed point in the model airframe (to eliminate the impact of gravity centre location). Here, the model nose tip (most forward point on the model) is chosen as the reference location. In CFD, the solver calculates the local pressure and shear stress in each and every wall cell over the entire model surface. It then integrates the normal force and pitching moment generated by local pressures and shear stresses about the model nose tip. The location of centre of pressure (distance from the nose tip) is then

calculated by dividing the calculated pitching moment by the calculated normal force. In MAC, the pitching moment coefficient of the entire model is estimated as the sum of those of the individual model components; the nose, cylindrical midsection, afterbody, wings, tails and about any given point (here, the nose tip is input by the user). The normal force coefficient is estimated in the same manner. The location of centre of pressure is then estimated by dividing the pitching moment coefficient by the normal force coefficient. In all three approaches, the resulting centre of pressure location (which is the distance to the centre of pressure measured from the model nose tip) is normalized with respect to the predefined reference length of the model (here, the model total length).
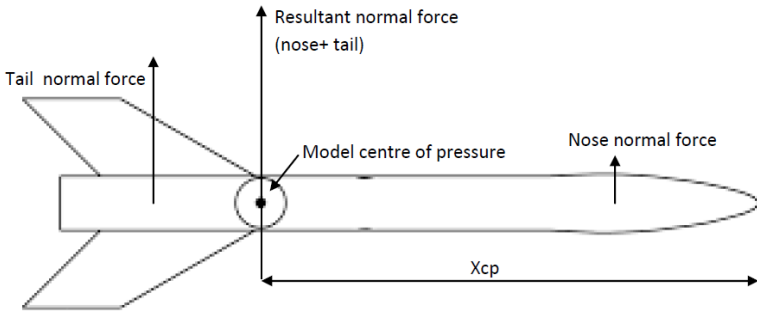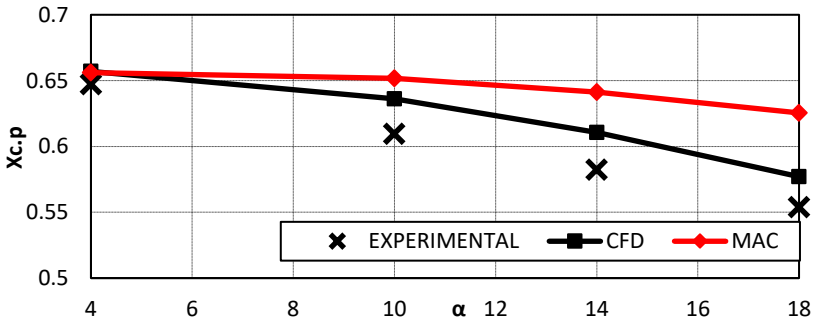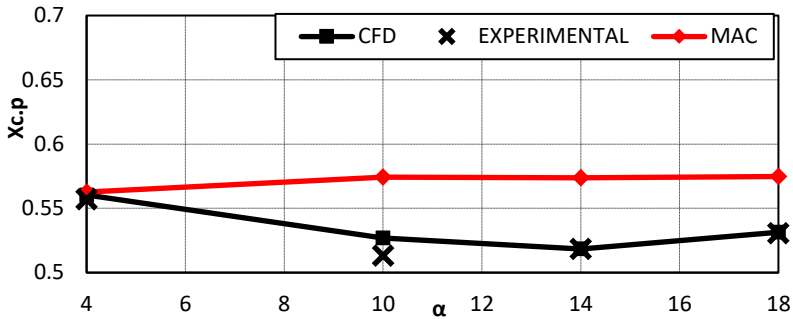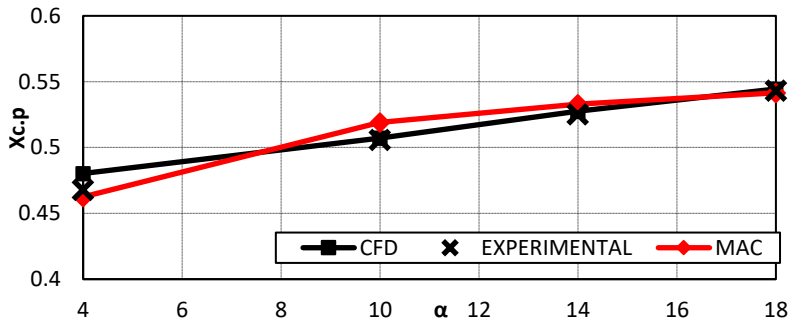

Figure 8: Location of model centre of pressure

The change in centre of pressure location with the freestream conditions is shown in Figure 9. The centre of pressure distance measured from the model nose tip is normalized with respect to the model length.

(a) Mach 1.5

(b) Mach 2.5

(c) Mach 4

Figure 9: Variation of normalized centre of pressure with incidence

At Mach 1.5, the measured normalized centre of pressure shifts forward with the increase of the angle of attack. CFD results show the same trend with a small error while a less steep trend is shown in MAC results. As the incidence angle increases from 4° to 18°, the drag coefficient drops by about 14.3%, 12%, and only 4.7% according to experimental, CFD, and MAC approaches, respectively. At Mach 2.5 and 3, a different behavior now appears from the CFD in a good agreement with the experimental measurements. The empirical technique does not show the same trend. Experimental measurements and CFD simulations predict a drop in drag coefficient by about 7% as the incidence angle increases from 4° to 14° followed by a 3% increase as the angle increases to 18°. In contrast, MAC predicts a small drag rise of 2% as the incidence angle increases from 4° to 14° then remains almost unchanged as the angle increases to 18°. Finally, at Mach 3.5 and Mach 4, the normalized centre of pressure shifts downstream with the increase in the angle of attack. This is valid for the data obtained from experimental measurements, CFD results, and MAC results. Overall, with reference to measurements, CFD results seem to be more accurate than the empirical ones in predicting both trend and values of the

model pressure centre location. Figure 10 aggregates the dependence of model pressure center location on the flight conditions namely, Mach number and incidence angle. The attitude of moving backward beyond Mach 3 for 10° incidence, beyond Mach 2.5 for 14° incidence and Mach 2 for 18° incidence is exclusively captured by CFD simulations in agreement with wind tunnel measurements. MAC slightly manages to capture the same attitude with less accurate values.

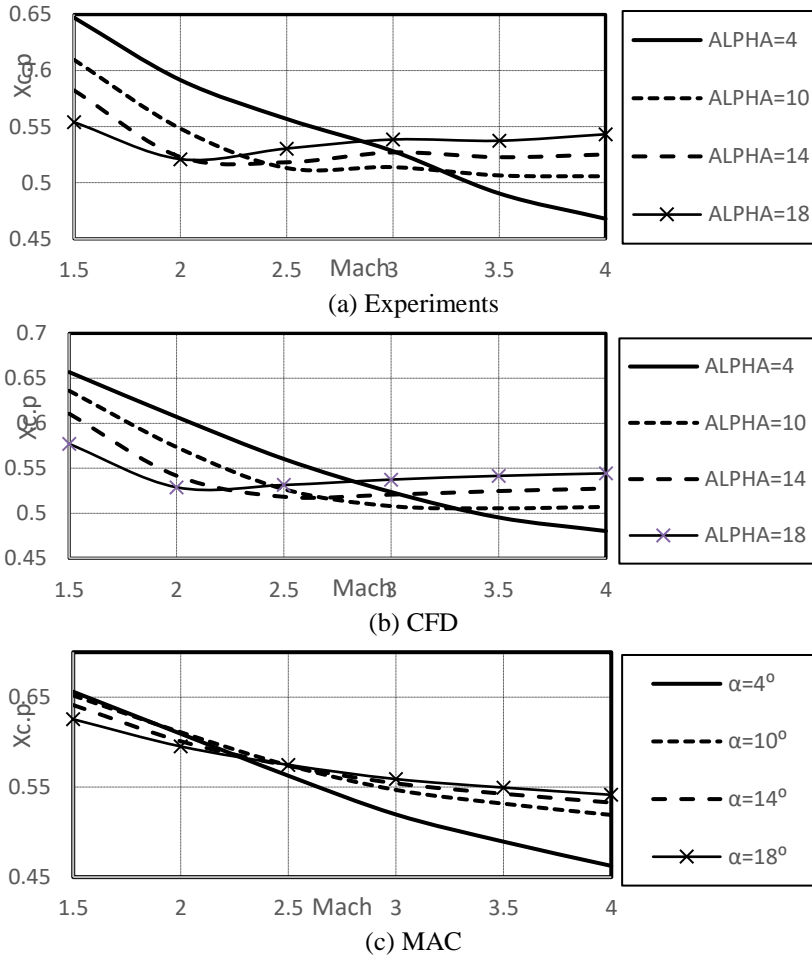(a) Experiments

(b) CFD

(c) MAC

Figure 10: Variation of center of pressure position with the Mach number and angle of attack

An explanation for the trend of centre of pressure location shown by both experimental measurements and CFD simulations is attempted here. At low Mach number and low incidence values, the centre of pressure location follows the typical trend namely, shifting upstream towards the missile nose with the increment of both Mach and incidence. As the Mach and/or incidence values increase, the centre of pressure shifts downstream rather than upstream. This may indicate the creation of a new component of normal force that acts on the aft 0f the missile causing the location of the resultant force to shift towards the missile base. This new component is the normal force due to separation of the cross flow around the missile midsection which gets more pronounced closer to missile base and as the cross flow speed (component of freestream velocity normal to the missile axis) increases. Hence, as inferred from Figure 10, the higher the freestream Mach value, the lower the incidence angle beyond which this phenomenon takes place. This explanation will be supported as the flow structure is investigated in the next section.

Evolution of the Flow Pattern with the Freestream Conditions

Results of numerical simulation are implemented to illustrate the evolution of the flow structure around the model with the freestream conditions. As a start, the freestream conditions at M=1.2 and α=4º are considered. The pressure and Mach contours in the symmetry plane of the domain around the model at these conditions are shown in Figure 11.

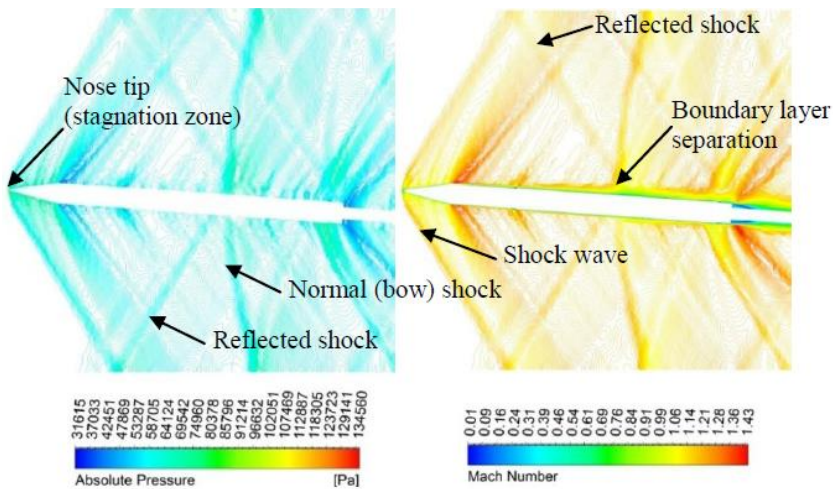Figure 11: Pressure and Mach contours around the model at M=1.2 and α =4º

As shown in the above figure, the region of maximum pressure is at windward side of the nose tip; the stagnation zone where the flow at this zone is of near-zero velocity. A shock is constructed at the nose tip extending to the walls of the test section and reflecting back. Behind the shock, there exists a region of higher pressure (than that before the shock) that is reduced again at the nose shoulder due to the expansion. Another local shock is created at leading edge of the upper and lower ducts. Finally comes the region of lowest pressure at the base due to the expansion fan then the wake behind the base. The reflected shock impinges back the model surface at the midsection of the model forming a region of high pressure after the reflected wave, which causes the boundary layer to separate forming a local normal shock (bow shock).The pressure and Mach contours in the symmetry plane of the domain around the model at M=1.5 and α=4° is shown in Figure 12.
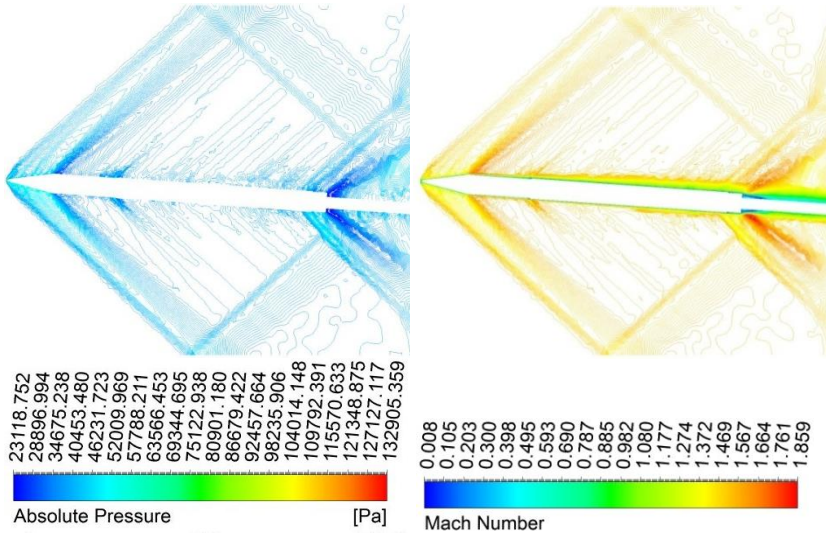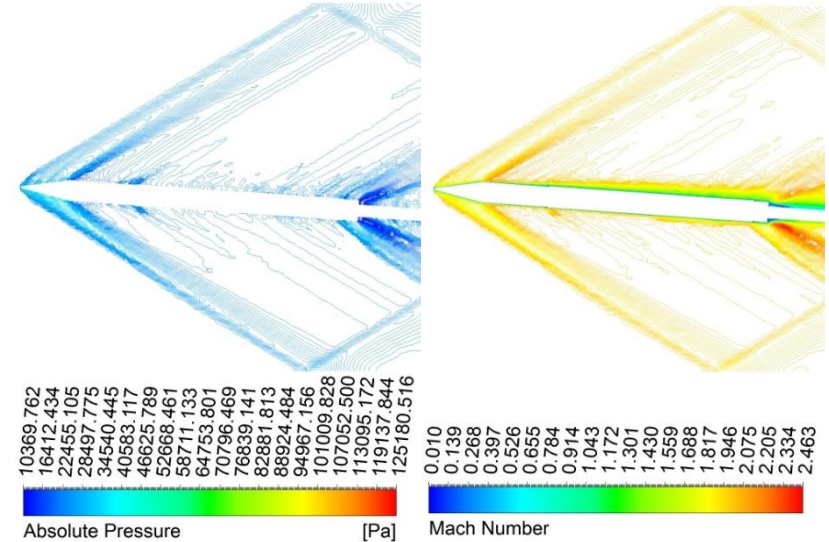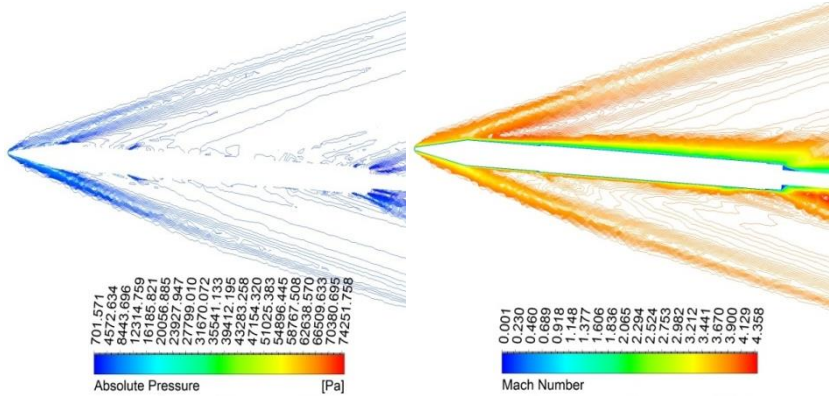

Figure 12: Pressure and Mach contours around the model at M=1.5 and α =4°

At Mach 1.5 the reflected shock intersects with the expansion at the base. This is more pronounced at the windward side. The expansion at the base is also followed by the recirculation of the confined air behind the base of the model. The boundary layer thickness appears to be increasing as the flow progresses towards the base of the model, and is larger on the leeward side than on the windward side of the model. The set of graphs in Figure 13 below illustrates the evolution of the flow pattern around the model with the rise of freestream Mach number. Pressure contours and Mach contours on the symmetry plane are shown to the left and right respectively.

(a) Mach 2

(b) Mach 4

Figure 13: Pressure and velocity contours around the model at α =4

As the Mach number increases, all shock waves and expansion fans become more oblique. The shock reflection shifts towards the exit of the test section such that eventually no shock reflection at all within the test section can be addressed starting from Mach 3. The evolution of the flow pattern as the incidence angle increases for Mach 1.5 freestream is illustrated in Figure 14 below.

(a) α =4⁰

(b) α =10⁰
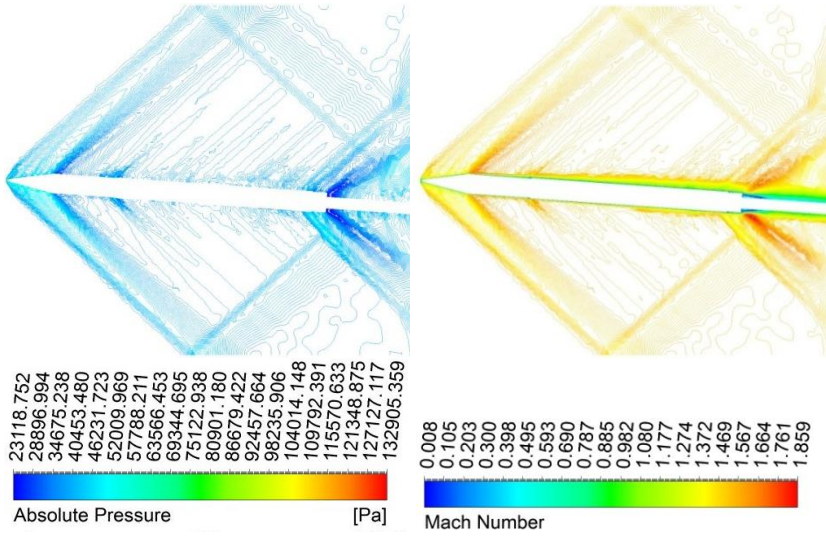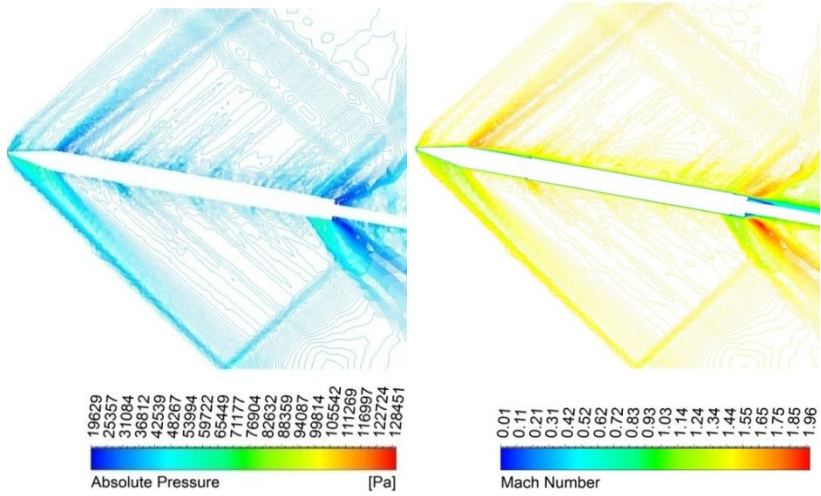
(c) α=18⁰
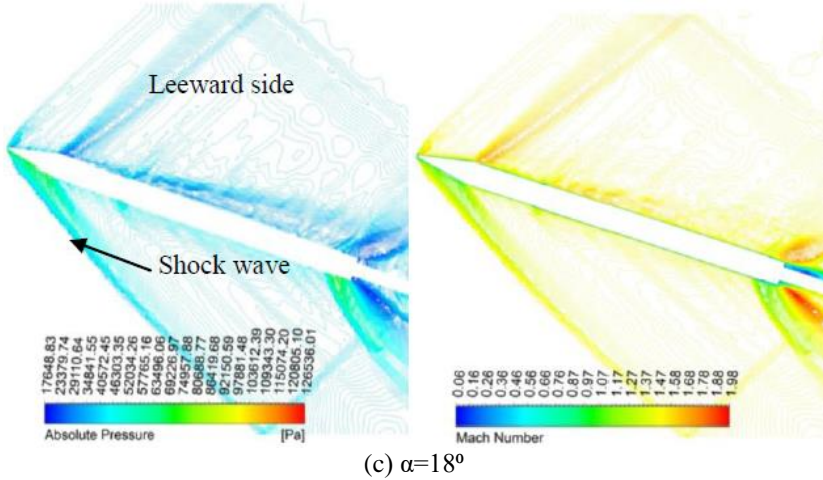
Figure 14: Pressure and Mach contours around the model at M=1.5

As the angle of attack increases, the flow deflection angle on the leeward side decreases while that on the windward side increases. Eventually, for incidence greater than 10⁰, the deflection angle at the leeward side is less than the angle of attack at which moment the shock occurs only at the windward side of the nose while an expansion takes place on the leeward side. Figures 15 and 16, respectively, show the cross flow pattern at the two stations namely, midway along the model and within the fin section.

(a) 4⁰ incidence   (b) 18⁰ incidence
Figure 15: Mach contours midway along the model at Mach 2

| (a) 4° incidence | (b) 18° incidence |

Figure 16: Mach contours at the wing-section of the model at Mach 2
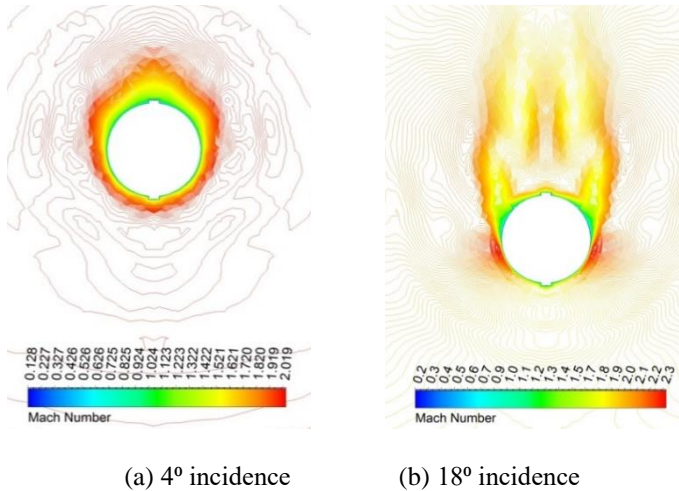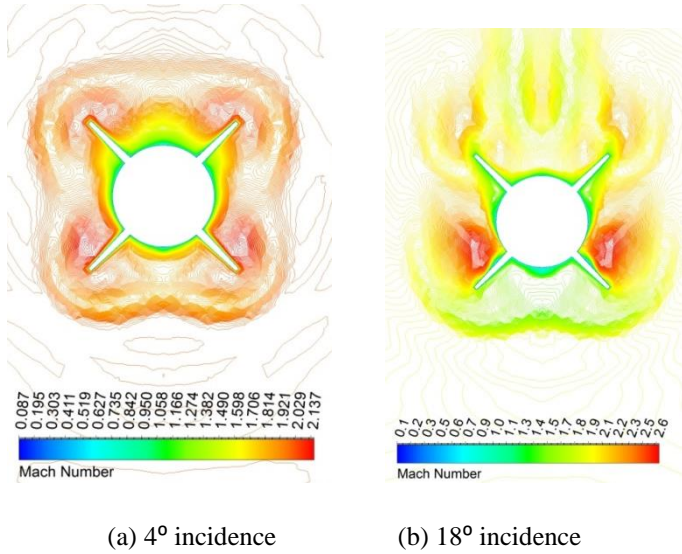
The figures above illustrate the flow pressure and velocity difference between the leeward and windward sides of the model, as explained before. This difference increases with the increase in incidence. In addition, as the incidence increases, the separation of the flow occurs earlier than that at lower incidences. The size of flow separation at the mod section, Figure 14a increases as the incidence angle increases. This feature supports the explanation stated earlier regarding the downstream shift of the missile centre of pressure location.

Conclusions

The aerodynamic characteristics of the modified configuration of a fin-stabilized missile are investigated in the present work and the objective is threefold. First, to compare the capabilities of prediction and accuracy of missile aerodynamic coefficients using three approaches namely experimental, computational, and empirical in the range of Mach numbers 1.5 to 4 and incidence angles 4° to 18°. Secondly, to assess the accuracy of the developed empirical code. Finally, to explore the flow features around the missile at this range of Mach numbers and angles of attack.

Referring to the results section, it can be seen that CFD results are closer to the measured values especially for drag and centre of pressure. In lift, the MAC tool provides highly acceptable accuracy with regard to its simplicity.

Overall, the accuracy of MAC improves as the incidence angle and Mach values increase. This invokes revising the empirical techniques used by MAC regarding especially the low Mach values and viscous cross flow calculations.

It has been proved, in many ways, that the location of pressure centre of the missile investigated shows a special behaviour. At low incidence, as the Mach number increases, the centre of pressure shifts towards the model nose. At higher incidence angles, as the Mach number increases, the pressure centre shifts upstream (towards the model nose) and then downstream. The value of the freestream Mach number beyond which the pressure centre location starts to migrate downstream decreases as the incidence angle increases. This behaviour of pressure centre location has been captured by experimental measurements, CFD simulations, and MAC. For the case investigated, the presence of wind tunnel test section wall had no interference on the flowfield around the model. The shock waves and expansion fans reflected on these walls yielding no effect on the measured aerodynamic parameters as long as they do not impinge back on the model.

References

[1]   F. A. Woodward, "Analysis and design of wing-body combinations at subsonic and supersonic speeds," *Journal of aircraft,* vol. 5, pp. 528-534, 1968.

[2]   W. C. Y. Oberkamp and J. C. Y. Nicolaides, "Aerodynamics of finned missiles at high angle of attack," *AIAA journal,* vol. 9, pp. 2378-2384, 1971.

[3]   W. Blake, "Missile Datcom- Applications to projectiles," in *AIAA Atmospheric Flight Mechanics Conference, Boston, MA*, 1989, pp. 212-221.

[4]   E. H. Smith, S. K. Hebbar, and M. F. Platzer, "Aerodynamic characteristics of a canard-controlled missile at high angles of attack," *Journal of spacecraft and rockets,* vol. 31, pp. 766-772, 1994.

[5]   J. White, "An assessment of missile DATCOM prediction accuracy relative to generic Body+ Wing+ Tail missile pitch aerodynamics," *AIAA paper,* pp. 95-1893, 1995.

[6]   F. Moore and T. Hymer, "Improved methodology for axial force prediction at angle of attack," *Journal of Spacecraft and rockets,* vol. 35, pp. 132-139, 1998.

[7]   Habip and A. Mehmet, "Prediction of Aerodynamic Characteristics of Missiles with Circular and Noncircular Cross Sections," *Turkish Journal of Engineering and Environmental Sciences,* vol. 23, pp. 149-160, 1999.

[8]   E. J. Abney and M. A. McDaniel, "High angle of attack aerodynamic predictions using missile datcom," *AIAA,* vol. 5086, p. 2005, 2005.

[9]   T. J. Sooy and R. Z. Schmidt, "Aerodynamic predictions, comparisons, and validations using missile Datcom (97) and aeroprediction 98 (AP98)," *Journal of spacecraft and rockets,* vol. 42, pp. 257-265, 2005.

[10]   Lesieutre, D. J., " Nonlinear Aerodynamic Predictions of Aircraft and Missiles Employing Trailing-Edge Flaps," Proceedings of the 52nd Aerospace Sciences Meeting, *AIAA Paper 2014-0055,* 2014.

[11]   Martinez, M., " Preliminary Aeromechanical Design of Sub-Guided Munition for Artillery Rockets," Proceedings of the 29th International Symposium on Ballistics, 9-13 May, Edinburgh, Scotland, 2016.

[12]   Doyle, J. B. and Rosema, C. C., "Improved Validation Methodology for Missile Datcom Development," AIAA paper 2011-1241, January 2011.

[13]   Maurice, A. F., "Aerodynamic performance predictions of a SA-2 Missile using Missile Datcom," Master Thesis, Naval Postgraduate School, Monterey, California, 2009

[14]   O. Baysal, K. Fouladi, and D. Miller, "Computations of supersonic flows over a body at high angles of attack," *AIAA journal,* vol. 27, pp. 427-437, 1989.

[15]   T. Birch, D. Ludlow, N. Qin, and B. DERA, "Towards an efficient, robust and accurate solver for supersonic viscous flows," in *Proceedings of the ICAS 2000 Congress, Harrogate, UK*, 2000.

[16]   J. Sahu, K. Heavey, and S. Dinavahi, "Application of CFD to high angle of attack missile flow fields," *Chimera,* vol. 10, p. 11, 2000.

[17]   S. B. Khelil, P. Guillen, M. Lazareff, and R. G. Lacau, "Numerical simulation of roll induced moment of cruciform tactical missiles," *Aerospace Science and Technology,* vol. 5, pp. 109-124, 2001.

[18]   S. Deck, P. Duveau, P. d'Espiney, and P. Guillen, "Development and application of Spalart–Allmaras one equation turbulence model to three-dimensional supersonic complex configurations," *Aerospace Science and Technology,* vol. 6, pp. 171-183, 2002.

[19]   J. DeSpirito, M. Vaughn, and W. D. Washington, "CFD Investigation of Canard-Controlled Missile with Planar and Grid Fins in Supersonic Flow," *AIAA paper 2002-4509,* 2002.

[20]   X. Liu and S. Fu, "Numerical simulation of compressible separated turbulent flows over inclined slender body," *Journal of spacecraft and rockets,* vol. 42, pp. 572-575, 2005.

[21]   H. H. Al-Kayiem, A. K. Hussein, J. M. Jaleel, and S. H. Hussain, "Numerical Computation of 3-dimensional Supersonic Flow Field over Seamless Missiles," *Indian Journal of Science and Technology,* vol. 7, pp. 1563-1572, 2014.

[22]   Yang, L., Wang, M., and Gao, Z., "Numerical Investigation of Unsteady Aerodynamic Characteristics of a Pitching Missile," Aerospace Science and Technology, Vol. 15, Issue 2, pp. 129-136, 2011.

[23] Ridluan, "CFD Investigation of Compressible Low Angles of Attack Flow over the Missile," *Journal of Physical Science and Application,* vol. 4, pp. 339-347, 2014.

[24] C. Rosema, E. Abney, S. Westmoreland, and H. Moore, "A Comparison of Predictive Methodologies for Missile Configurations with Strakes," in *33rd AIAA Applied Aerodynamics Conference*, 2015.

[25] ANSYS Fluent 14.5.7, User Guide.

[26] DSSC, "Technical Report DSSC-TR70120," 2012.

[27] O. E. A. Hamid, "MAC user guide," Generalized MAC ed, EAF-TRC, 2004.

[28] Lebejev, A. A. and Cherrobrovky, P. S., "Flight Dynamics," Machinestroj, Moskow, 1973

[29] Krasnov, N.R., "Aerodynamics," Mir Publisher, Moskow, 1985

[30] Rayiner, D., "Aircraft Design, A conceptual Approach," AIAA Educational Series, 1989.

[31] "U.S.A.F Stability and Control DATACOM," MacDonnel Douglas Corporation, 1975.

[32] V. Broz, 'Aerodynamic Derivatives of Airplanes in Transonic Flow," Czechoslovak Aeronautical Research centre (VZLV), Prag 1966.

[33] M. Dauek, "Aerodynamic and Flight Dynamics of Guided Missiles," VAAZ, Brno, 1964.